NANO LETTERS

pubs.acs.org/NanoLett Letter

Low-Dissipation Nanomechanical Devices from Monocrystalline Silicon Carbide

Leo Sementilli, Daniil M. Lukin, Hope Lee, Joshua Yang, Erick Romero, Jelena Vučković,* and Warwick P Bowen

Cite This: https://doi.org/10.1021/acs.nanolett.4c06475 Read Online

ACCESS | Metrics & More | Article Recommendations | Supporting Information

ABSTRACT: The applications of nanomechanical resonators range from biomolecule mass sensing to hybrid quantum interfaces. Their performance is often limited by internal material damping, which can be greatly reduced by using crystalline materials. Crystalline silicon carbide is appealing due to its exquisite mechanical, electrical, and optical properties, but has suffered from high internal damping due to material defects. Here we resolve this by developing nanomechanical resonators fabricated from bulk monocrystalline 4H-silicon carbide. This allows us to achieve damping as low as 2.7 mHz, more than an order-of-magnitude lower than any previous crystalline silicon carbide resonator and corresponding to a quality factor as high as 20 million at room temperature. The volumetric dissipation of our devices reaches the material limit for silicon carbide for the first time. This provides a path to greatly increase the performance of silicon carbide nanomechanical resonators.

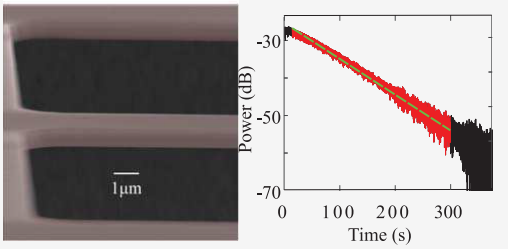

KEYWORDS: *nanomechanical resonators, mechanical dissipation, monocrystalline silicon carbide*

I. INTRODUCTION

Nanomechanical resonators have many applications, from nanoscale probes in biological environments[1,2] to radio and microwave frequency timing[3,4] and on-chip navigation and position awareness.[5,6] The mechanical dissipation rate is a key figure of merit.[7] It is ultimately determined by material friction and dictates the sensitivity limits of nanomechanical sensors, accuracy of nanomechanical timing, and sharpness of nanomechanical filters. In principle pure crystalline materials have lower material dissipation than amorphous counterparts because of their ordered atomic lattice. However, defects introduced during material growth, processing, and nanofabrication often result in dissipation rates higher than those of amorphous materials.[8,9]

Crystalline silicon carbide (SiC) is an important material for nanomechanics, as it possesses many attractive mechanical, electronic, and optical properties. It has high material yield strength, can be fabricated into high-stress thin films,[8,10−12] has high thermal conductivity and wide electronic bandgap,[13] and hosts color centers used for quantum photonics.[14,15] Furthermore, it has excellent photonic properties,[16−18] can be mass manufactured in industrial settings, and is sold as an affordable semiconductor. However, to date, all crystalline silicon carbide nanomechanical resonators have had material dissipation orders-of-magnitude higher than the predicted volumetric limit.[8,12,19,20]

Here, we develop crystalline silicon carbide nanomechanical devices with ultralow dissipation, utilizing bulk sublimation grown silicon carbide crystals and a grind-and-polish technique to achieve defect-free thin films. This eliminates the interfacial defect layer that causes dissipation in silicon carbide nanomechanical resonators fabricated directly on silicon substrates.[8,12] We observe greatly reduced intrinsic damping, achieving dissipation rates as low as 2.7 mHz at room temperature. This is nearly two orders-of-magnitude lower than what has been achieved in bulk crystalline silicon carbide resonators,[21] an order-of-magnitude lower than silicon carbide nanomechanical resonators fabricated from heteroepitaxially grown crystals,[8] and a factor of 1.6× better than the best reported in high-stress amorphous silicon carbide resonators.[22] It corresponds to a quality factor as high as 20 million, even with only a few hundred megapascal of tensile stress. Fabrication from bulk silicon carbide allows us to reach volumetric dissipation at the reported material limit.[23,24]

The low linear dissipation allows us to make the first observation of nonlinear dissipation in crystalline silicon carbide nanomechanical resonators. We find that this is lower than other materials such as amorphous silicon nitride. This is important for applications where nonlinear effects constrain performance, such as mass sensing[25,26] and nanomechanical computing.[27,28]

Received: December 17, 2024
Revised: February 25, 2025
Accepted: March 31, 2025

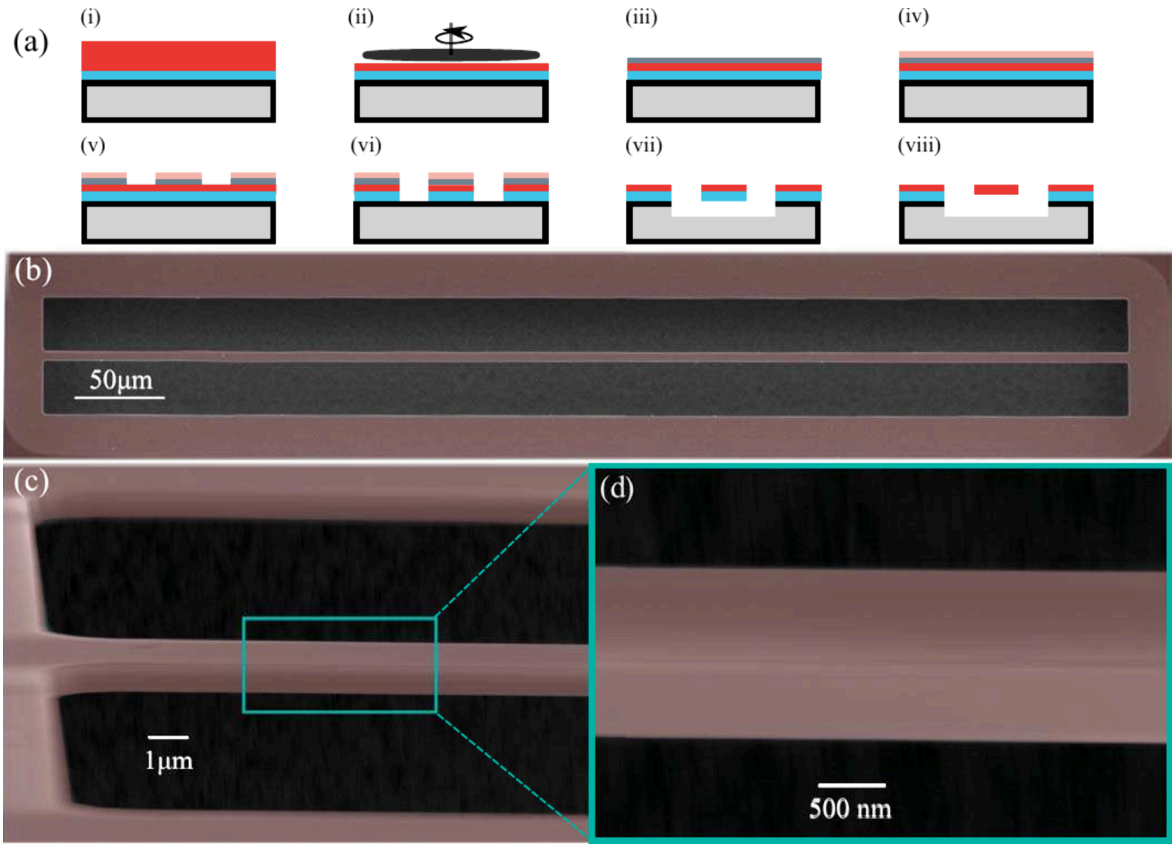

Figure 1. (a) Fabrication process. Colors correspond to red, SiC; light blue, SiO_2; dark gray, aluminum; salmon, resist; light gray, silicon substrate. (b) SEM image of a nanostring resonator made of 4H-SiC. (c) SEM image of the sidewall and clamping point of a nanostring resonator. (d) Higher magnification SEM image of a nanostring sidewall from (c). Minimal surface roughness is observed in SEM images taken with a 10 kV accelerating voltage and 17 k magnification.

At the material damping limit and when strained to near the material yield strength (21 GPa[10]), crystalline silicon carbide resonators could allow quality factors exceeding 10 billion at room temperature. This would surpass the achievable quality factors of other materials, such as silicon and silicon nitride, which are currently limited by higher intrinsic nanomechanical dissipation and lower yield strengths.[7,10,29−31] Realizing such extreme nanomechanical quality factors at room temperature, while challenging, may shed light on new dissipation mechanisms and enable fundamentally new applications such as nanomechanical tests of spontaneous wave function collapse,[32] sensing of dark matter,[33] and room-temperature quantum optomechanics.[31,34]

II. DEVICE FABRICATION

The devices studied here are fabricated using a process consisting of thin film preparation, metal deposition, electron beam patterning, reactive ion etching, and dry selective release following the process outlined in ref 17 (see Figure 1(a)). The samples are first derived from bulk crystalline 4H-SiC wafers, which are then thermally bonded onto silicon carrier wafers via a thin (160 nm) bonding silicon oxide layer. The bonding procedure requires annealing at high temperatures (900 °C),[17] which introduces stress into the SiC layer upon thermalization to room temperature. The magnitude of this stress is determined by the difference in thermal expansion coefficients between silicon and silicon carbide. The bonded SiC film is then thinned to submicron thickness using the grind-and-polish technique.[17] This technique, developed in recent years, has been used to enable low-loss integrated photonics in 4H-SiC and diamond,[17,35] as well as, most recently, on-chip titanium-sapphire lasers.[36] The thinning process results in a thickness nonuniformity of approximately 10−20 nm per millimeter of resonator length across our sample, which we determine using optical thin film profiling techniques. To account for this, mechanical resonators are selectively patterned within regions of largest mapped uniformity. The mean device thickness is then found across each resonator's footprint and used for analysis purposes.

After the preparation of the crystalline thin film, aluminum is evaporated on the SiC layer to act as a hard mask for etching. Following this, device geometries are initially realized using electron beam lithography, then formed using reactive ion etching of the aluminum, SiC, and silica layers. The aluminum is then stripped chemically, and the devices are undercut using XeF_2 dry etching. This leaves 4H-SiC structures suspended with thermal silica still adhered to the bottom interface of the devices. The remaining thermal silica is then removed using vapor HF, resulting in freestanding structures that are purely 4H-SiC.

We focus our experiments on tensile stressed high-aspect-ratio nanostring resonators, which inherently possess large dissipation dilution factors that allow quality factors far above material loss limits[37−39] and are amenable to analytical modeling.[7,24] SEM images of a completed nanostring are presented in Figures 1(b−d). Within these images, both the device's top surfaces and sidewalls appear relatively smooth. To quantify surface roughness, we perform a spatial

https://doi.org/10.1021/acs.nanolett.4c06475
Nano Lett. XXXX, XXX, XXX−XXX

autocorrelation on a section of the resonator's vertical sidewall in Figure 1(d). From this, we observe roughness correlations on the length scale of 6 nm, which both sets a limit to surface feature sizes we can detect with SEM and speaks to the extent of observable roughness in our device sidewalls.

III. RESULTS

We characterize the dissipation and quality factors of the nanomechanical resonators using ringdown measurements in an optical heterodyne detection setup.[8,12] We perform ringdown measurements for the first three transverse modes of 20 high-aspect-ratio nanostring devices with lengths (L) of 3.1 mm and thicknesses (h) between 110 and 135 nm.

An example experimental ringdown measurement on a nanostring with a resonance frequency of 53 kHz is shown in Figure 2(a). It provides a quality factor of $Q = 1.5 \times 10^7$. The

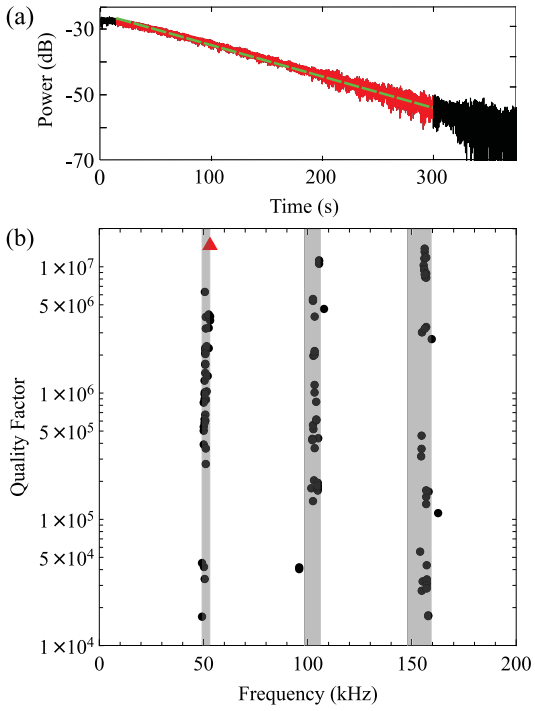

Figure 2. (a) Ringdown measurement of a device with a quality factor exceeding 10^7 at 53 kHz. (b) $Q{\cdot}f$ map for the first three transverse modes of 20 high-aspect-ratio nanostrings. The shaded gray regions represent the expected frequency range based on device dimensions and tensile stress. The red-colored point represents the measurement shown in (a).

measured quality factors for the first three transverse mechanical modes of all 20 devices are plotted in Figure 2(b) as a function of resonance frequency. Quality factors exceeding 10^7 are observed for all three modes. The gray shaded regions represent the expected eigenfrequency range for the first three transverse mechanical modes (n = 1, 2, 3) based on the analytical expression[24]

$$f = \frac{n}{2L}\sqrt{\frac{\sigma}{\rho}} \tag{1}$$

where σ is the stress and ρ = 3.2 g/cm^3[40] is the material density. We find that the stress of the devices range from σ = 290 MPa to 335 MPa from the measured minimum and maximum fundamental resonance frequencies. Extrapolating this range to the second and third resonances, we find good agreement between theory and experiment (gray bounds in Figure 2(b)).

The mechanical dissipation rate of each mode can be determined as $\Gamma/2\pi = f/Q$. We find a minimum mechanical dissipation rate of 2.7 mHz, achieved for the fundamental transverse mode of a high-aspect-ratio nanostring (observed from nonlinear characterization later in Section IV). This is the lowest dissipation rate reported for any silicon carbide mechanical resonator to date. It is more than an order-of-magnitude better than the best reported previously in crystalline 3C-SiC nanostrings.[37] The lower dissipation realized here can be largely attributed to the thin film preparation technique allowing high quality crystalline resonators, but also in part to the larger device aspect ratio realized in this work.[37] Despite the significant reduction in the dissipation of crystalline SiC resonators, our results are only marginally better (1.66×; see Table 1) than the lowest

Table 1. Comparison of Silicon Carbide Nano/Bulk Mechanical Resonators[a]

Ref	Frequency	Q (×10^6)	$\Gamma/2\pi$ (mHz)	Type
21	5.3 MHz	18	290	4H-SiCOI bulk
22	895 kHz	198	4.5	amorphous SiC nano
8	211 kHz	1.74	121	3C-SiC nano
12	280 kHz	2.9	90	3C-SiC nano
this work	53 kHz	20	2.7	4H-SiCOI nano

[a]All measurements are at room temperature. For direct comparison of intrinsic quality factors see Figure 3.

dissipation rate achieved in amorphous SiC resonators.[22] However, to achieve low dissipation, ref 22 employed soft-clamping techniques and higher stress than our work. Applied into crystalline SiC resonators, these techniques have potential to further reduce dissipation beyond the values we report.

While 4H-SiC resonators provide exceptionally low dissipation, the current fabrication procedure results in five times less tensile stress than previous silicon carbide devices in the literature.[37] Hence, one would expect lower quality factors and $Q{\cdot}f$ values than previous demonstrations, since both dissipation dilution factors and frequency increase with tensile stress.[7,24] Despite this, our highest measured quality factor of 20 million at room temperature is nearly an order of magnitude higher than the best reported for crystalline SiC nanostring and trampoline nanomechanical resonators in the literature.[8,19,37] Furthermore, our best $Q{\cdot}f$ product of 1×10^{12} in these devices exceeds the highest reported $Q{\cdot}f$ product in high-stress (σ = 1.5 GPa) crystalline 3C-SiC nanostrings.[12] The high $Q{\cdot}f$ product despite low device stress demonstrated here challenges the standard approach where high stress is utilized to increase both resonance frequency and quality factors.[7,24]

To form an understanding of intrinsic dissipation mechanisms in 4H-SiC, we combine the quality factor measurements of high-aspect-ratio nanostrings, together with a suite of ringdown measurements from 18 other cantilever resonators and 30 low-aspect-ratio nanostrings (see Supporting Information). The additional resonator geometries are needed to separate the contributions of surface and volumetric effects toward the total intrinsic material dissipation. Cantilever resonators possess no tensile stress and low radiation loss

https://doi.org/10.1021/acs.nanolett.4c06475
Nano Lett. XXXX, XXX, XXX−XXX

(see Supporting Information); therefore their measured quality factors well approximate the intrinsic quality factor, Q_{int}, of the material.[8,24,29] String resonators possess tensile stress and dissipation dilution, as well as non-negligible radiation loss. Therefore, the measured quality factors of string resonators do not exactly reflect the intrinsic quality factor. In order to calculate the intrinsic quality factor of each high- and low-aspect-ratio nanostring, we determine its dissipation dilution factor using the analytical expression[24,41]

$$D \approx \left[\frac{(n\pi)^2}{12}\frac{E}{\sigma}\left(\frac{h}{L}\right)^2 + \frac{1}{\sqrt{3}}\sqrt{\frac{E}{\sigma}}\left(\frac{h}{L}\right)\right]^{-1} \quad (2)$$

where E = 440 GPa is the Young's modulus of 4H-SiC.[42] Using eq 2 and the relationship between intrinsic quality factors and dissipation diluted quality factors ($Q_D = Q_{int} \times D$), we extract an intrinsic quality factor for nanostring resonators of

$$Q_{int} = (D \times (Q_D^{-1} - Q_{rad}^{-1}))^{-1} \quad (3)$$

where Q_{rad} is the radiation loss limited quality factor (see Supporting Information).[8] We include this loss mechanism for all high- and low-aspect-ratio nanostrings, using each device dimension and intrinsic stress inferred from the fundamental transverse eigenfrequency.

We plot the extracted intrinsic quality factors for all high- and low-aspect-ratio nanostrings alongside our cantilever quality factors in Figure 3. More than 20 devices have intrinsic

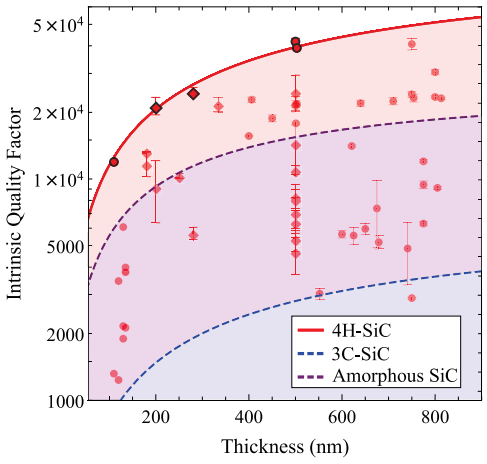

Figure 3. Cumulative extracted intrinsic quality factors for all devices. Each nanostring is represented by a red circular point, and each cantilever is represented by a red diamond. We fit the upper bounds of our extracted intrinsic quality factors (5 red points with black borders) as a function of thickness using eq 4, and the fitting parameter α accounting for radiation loss in nanostring resonators, and plot it using a red line. We add Q_{int} models for amorphous (dashed purple) and crystalline 3C-SiC (dashed blue) for comparison.[8,22]

quality factors above 10^4, including at least one device from each of the three sample sets. The maximum intrinsic quality factor from the data is 4.2×10^4 in a 500 nm thick nanostring resonator. No significant differences are observed between the intrinsic quality factors of cantilever and string geometries. This is expected, as intrinsic quality factors are primarily determined by a resonator surface-to-volume ratio rather than resonator type.[24] This indicates that the dissipation dilution and radiation loss models of nanostring resonators are appropriate for all nanostrings measured. The intrinsic quality factor increases with device thickness. This is anticipated since surface losses become less important as the surface area to volume ratio of the devices decreases. Similar dependence has been commonly observed in silicon nitride[29] and other nanomechanical resonators.[8,30,43]

To determine the upper limit of the intrinsic quality factor, a least-squares fit is performed among the five red data points with black boundaries in Figure 3. We choose these five points because they represent the highest measured intrinsic quality factors at different device thicknesses. They therefore provide information about the highest intrinsic quality factors achieved for the 4H-SiC nanomechanical resonators in this study. The least-squares fit follows the process from ref 8 using the standard nanomechanical volume and surface dissipation model given by[24,29]

$$Q_{int}(h) = (Q_{vol}^{-1} + (Q_{surf} \cdot h)^{-1})^{-1} \quad (4)$$

with an additional fitting parameter α, which accounts for radiation loss of nanostring resonators (see Supporting Information). It is plotted as the red line in Figure 3 and yields $Q_{vol} = 1.5 \times 10^5$, $Q_{surf} = 11.5 \times 10^{10}$ m^{-1}·h, and α = 317. From it, we find that surface loss becomes the dominating intrinsic loss mechanism at roughly 1300 nm thickness.

The highest observed volumetric quality factor of our resonators is consistent with the theoretical material limit (1×10^5) based on the material loss tangent of silicon carbide.[23,24] We measure five devices at this material limit, representing 7.5% of our total devices measured. Across three different resonator geometries encompassing 68 total resonators, we find the likelihood that devices reach the material limit decreases as device footprint increases (see Supporting Information). This is expected under the assumption that the thin films have a uniform density of defects per area, and therefore larger devices will encounter more defects. We hypothesize that only partial regions of the thin films are effectively defect-free due to the introduction of local crystalline imperfections during thin film preparation.

IV. OBSERVATION AND QUANTIFICATION OF NONLINEAR DISSIPATION

For applications such as resonant mass sensing[25] and nanomechanical computing,[28] where the resonator is driven to high amplitudes, it is important to quantify not just linear dissipation but also nonlinear dissipation. The nonlinear dissipation has been characterized in high-stress amorphous silicon nitride,[44] but has yet to be determined in crystalline silicon carbide resonators. To determine it, we strongly drive our high-aspect-ratio nanostrings and conduct ringdown measurements as shown in Figure 4.

From this figure, it is apparent the experimental trace deviates from a standard linear decay (blue dashed line) at high amplitudes. To account for this, we include a nonlinear damping term into the ringdown model for dissipation-diluted nanomechanical resonators.[44] This allows us to extract the linear dissipation rate as well as the nonlinear damping loss parameter. We find the linear mechanical dissipation rate to be 2.7 mHz, a linearly damped mechanical quality factor of 2.0×10^7, and a nonlinear damping parameter of 1.1×10^{13} s^{-1} m^{-2}. The nonlinear damping parameter is similar to but lower than the lowest that has been experimentally determined in silicon nitride resonators of similar thickness ($\approx 1.5 \times 10^{13}$–$1 \times$

https://doi.org/10.1021/acs.nanolett.4c06475
Nano Lett. XXXX, XXX, XXX−XXX

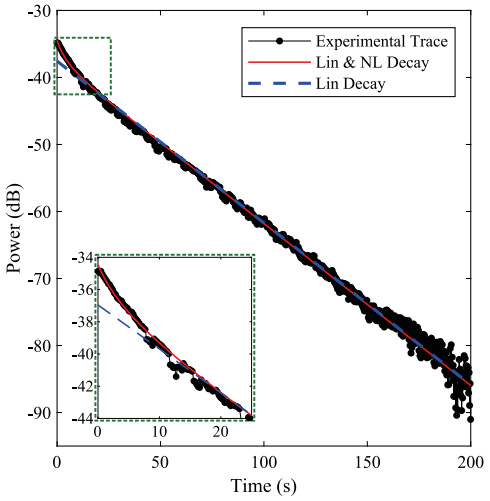

Figure 4. Ringdown measurement and analytical fits of a strongly driven, high-Q nanostring resonator. The black trace represents experimental data for the fundamental transverse mode of a high-aspect-ratio nanostring. The red trace represents the fit using a linear and nonlinear decay term.[44] The blue dashed trace represents the decay of a damped harmonic oscillator, used to fit the ringdowns of linear nanomechanical resonators.

$10^{16} s^{-1} m^{-2}$).[44] This suggests that 4H-SiC resonators may be more linear than those composed of silicon nitride, allowing improved performance.

V. COMPARISON WITH STATE-OF-THE-ART

To compare our results to current state-of-the-art devices in silicon carbide, we plot models of the intrinsic quality factor of 3C-SiC and amorphous SiC nanomechanical resonators in Figure 3 (dashed lines).[8,22] Using the parameters of these intrinsic quality factor models we find that the 4H polytype has a 23 times higher volumetric quality factor and 11 times higher surface quality factor compared to 3C-SiC. Interestingly, for the specific case when the interfacial defect layer is removed from 3C-SiC nanomechanical resonators, its surface loss agrees to within 5% of that found for 4H-SiC here.[8] However, even with the interfacial defect layer removed in 3C-SiC, its volumetric quality factor is still over an order-of-magnitude lower than that of 4H-SiC.[8] This suggests there is an additional cause, in addition to the defect layer, which is partly responsible for the difference in volumetric quality factors between 3C- and 4H-SiC. We speculate this may be related to the cubic versus hexagonal crystalline structure of each respective polytype but requires further study.

The 4H-SiC nanomechanical resonators from this work also outperform amorphous SiC, with 40% less surface damping and five times less volumetric damping.[22] While these comparisons are between the upper bounds of the intrinsic quality factor of each material, we measure many resonators with intrinsic quality factors above the limits of both crystalline 3C and amorphous silicon carbide (98% exceed the upper limit for 3C-SiC and 41% exceed it for amorphous SiC).

Compared to the highest reported values for silicon nitride resonators at room temperature, 4H-SiC possesses a volumetric quality factor five times larger and a comparable surface quality factor (4H-SiC is 15% greater).[29] Although the dependence of the nanomechanical quality factor on device thickness has not been fully characterized for crystalline silicon and diamond, we can compare measured total intrinsic quality factors for cantilever resonators of thicknesses between 100 and 300 nm to 4H-SiC. The intrinsic quality factor of 4H-SiC is roughly 35% higher than the best reported values for single-crystal silicon at room temperature.[30,45] It is about three times higher than that reported for polycrystalline diamond, but an order of magnitude less than electronic grade single-crystal diamond.[45] Applying surface treatments to single-crystal diamond nanomechanical resonators has shown to provide a three to ten times permanent reduction in surface loss.[45,46] Given the similar crystalline structures of diamond and 4H-SiC, it is conceivable that surface treatments of this kind could also be effective for 4H-SiC nanomechanical resonators.

Increasing the tensile stress to the material yield strength and using soft-clamped resonator geometries[47−49] could allow for quality factors of tens of billions at room temperature in 4H-SiC. Although challenging, if accomplished, this would be comparable to the best cryogenic results using strained silicon nanomechanical resonators at 7 K,[47] as well as the breathing mode of silicon nanomechanical resonators at millikelvin temperatures.[50]

VI. DISCUSSION

While this work reports the lowest dissipation rate achieved to date in a SiC nanomechanical resonator, much lower dissipation has been achieved in silicon nitride resonators due to effective soft-clamping of resonators and high stress.[49,51−53] A key difference between our results and this prior work is that ours is achieved with low stress. This has many practical advantages over highly stressed resonators which are more likely to fail in demanding real-world applications such as inertial and mass sensing.[5,26] Furthermore, it may be possible to reach far lower dissipation levels in crystalline SiC using surface treatments and alternative resonator geometries with higher stress and dissipation dilution such as hierarchical, polygon, and torsional resonators.[49,51,52] This requires two challenging advances in thin film development. Specifically, the grind-and-polish technique both needs to be successfully extended to films thinner than demonstrated here or in the literature[54,55] and needs to allow for higher tensile stress. Achieving much higher levels of tensile stress will likely require new approaches, similar to those developed for strained silicon-on-insulator wafers.[47,56]

Assuming the same resonator geometry and dimensions as ref 49, stressed to half of silicon carbide's yield strength,[10] predicts a diluted quality factor of 18 billion at room temperature. If realized, this would be comparable to the best reported cryogenic nanomechanical resonators.[47,50] The benefit of using crystalline SiC over other materials is due to both the lower intrinsic damping and higher material yield strength, which when implemented with a soft-clamped resonator allows dissipation dilution to scale proportionally with strain.[39,47]

■ ASSOCIATED CONTENT

Supporting Information

The Supporting Information is available free of charge at https://pubs.acs.org/doi/10.1021/acs.nanolett.4c06475.

Information on measurement setup, additional measurements and analysis, details on radiation loss calculation, additional analysis on rate of material limited devices,

https://doi.org/10.1021/acs.nanolett.4c06475
Nano Lett. XXXX, XXX, XXX−XXX

FEM modeling of the effect of overhang on dissipation dilution factors (PDF)

AUTHOR INFORMATION

Corresponding Author

Jelena Vučković − *E. L. Ginzton Laboratory, Stanford University, Stanford, California 94305, United States;* orcid.org/0000-0002-4603-9686; Email: jela@stanford.edu

Authors

Leo Sementilli − *The Australian Research Council Centre of Excellence for Engineered Quantum Systems, School of Mathematics and Physics, University of Queensland, St. Lucia, Queensland 4072, Australia;* orcid.org/0000-0001-7979-3530

Daniil M. Lukin − *E. L. Ginzton Laboratory, Stanford University, Stanford, California 94305, United States*

Hope Lee − *E. L. Ginzton Laboratory, Stanford University, Stanford, California 94305, United States;* orcid.org/0000-0003-3043-3459

Joshua Yang − *E. L. Ginzton Laboratory, Stanford University, Stanford, California 94305, United States*

Erick Romero − *The Australian Research Council Centre of Excellence for Engineered Quantum Systems, School of Mathematics and Physics, University of Queensland, St. Lucia, Queensland 4072, Australia*

Warwick P Bowen − *The Australian Research Council Centre of Excellence for Engineered Quantum Systems, School of Mathematics and Physics, University of Queensland, St. Lucia, Queensland 4072, Australia; The Australian Research Council Centre of Excellence in Quantum Biotechnology, School of Mathematics and Physics, University of Queensland, St. Lucia, Queensland 4072, Australia*

Complete contact information is available at: https://pubs.acs.org/10.1021/acs.nanolett.4c06475

Author Contributions

L.S. and D.M.L. contributed equally to this paper.

Notes

The authors declare no competing financial interest.

ACKNOWLEDGMENTS

This work was supported by the Australian Research Council Centres of Excellence for Engineered Quantum Systems (EQUS, CE170100009) and Quantum Biotechnology (QUBIC, CE230100021). The authors acknowledge the facilities, and the scientific and technical assistance, of the Australian Microscopy & Microanalysis Research Facility at the Centre for Microscopy and Microanalysis, The University of Queensland. This research is partially supported by the Commonwealth of Australia as represented by the Defence Science and Technology Group of the Department of Defence. The work at Stanford was supported by the Vannevar Bush Faculty Fellowship from the Department of Defense.

REFERENCES

(1) Chien, M.; Brameshuber, M.; Rossboth, B. K.; Schütz, G. J.; Schmid, S. *Proc. Natl. Acad. Sci. U. S. A.* **2018**, *115*, 11150.

(2) Rosłoń, I. E.; Japaridze, A.; Steeneken, P. G.; Dekker, C.; Alijani, F. *Nat. Nanotechnol.* **2022**, *17*, 637.

(3) Massel, F.; Heikkila, T. T., Pirkkalainen, J.-M.; Cho, S. U.; Saloniemi, H.; Hakonen, P. J.; Sillanpaa, M. A. *Nature* **2011**, *480*, 351.

(4) Nguyen, C. T.-c. IEEE Transactions on Ultrasonics, Ferroelectrics, and Frequency Control. *IEEE Transactions on Ultrasonics, Ferroelectrics, and Frequency Control* **2007**, *54*, 251.

(5) Krause, A. G.; Winger, M.; Blasius, T. D.; Lin, Q.; Painter, O. *Nat. Photonics* **2012**, *6*, 768.

(6) Fan, X.; Forsberg, F.; Smith, A. D.; Schröder, S.; Wagner, S.; Rödjegård, H.; Fischer, A. C.; Östling, M.; Lemme, M. C.; Niklaus, F. *Nature Electronics* **2019**, *2*, 394.

(7) Sementilli, L.; Romero, E.; Bowen, W. P. *Adv. Funct. Mater.* **2022**, *32*, 2105247.

(8) Romero, E.; Valenzuela, V. M.; Kermany, A. R.; Sementilli, L.; Iacopi, F.; Bowen, W. P. *Physical Review Applied* **2020**, *13*, 044007.

(9) Bückle, M. *Nanomechanical Systems Based on Tensile-Stressed Crystalline Indium Gallium Phosphide*; Ph.D. thesis (2020).

(10) Petersen, K. E. *Proceedings of the IEEE* **1982**, *70*, 420.

(11) Severino, A.; Locke, C.; Anzalone, R.; Camarda, M.; Piluso, N.; La Magna, A.; Saddow, S.; Abbondanza, G.; D'Arrigo, G.; La Via, F. *ECS Trans.* **2011**, *35*, 99.

(12) Kermany, A. R.; Brawley, G.; Mishra, N.; Sheridan, E.; Bowen, W. P.; Iacopi, F. *Appl. Phys. Lett.*, *6* (**2014**), DOI: 10.1063/1.4866268.

(13) Perret, R. *Power Electronics Semiconductor Devices*, 1st ed. (John Wiley & Sons, Ltd, 2009).

(14) Lukin, D. M.; Guidry, M. A.; Yang, J.; Ghezellou, M.; Deb Mishra, S.; Abe, H.; Ohshima, T.; Ul-Hassan, J.; Vučković, J. *Physical Review X* **2023**, *13*, 011005.

(15) Janitz, E.; Bhaskar, M. K.; Childress, L. *Optica 7*, 1232 (**2020**).

(16) Guidry, M. A.; Lukin, D. M.; Yang, K. Y.; Trivedi, R.; Vuckovic, J. *Nature Photonics* **2022**, *16*, 52

(17) Lukin, D. M.; Dory, C.; Guidry, M. A.; Yang, K. Y.; Mishra, S. D.; Trivedi, R.; Radulaski, M.; Sun, S.; Vercruysse, D.; Ahn, G. H.; Vuckovic, J. *Nature Photonics* **2020**. *14*, 330.

(18) Castelletto, S.; Boretti, A. *Journal of Physics: Photonics 2*, 022001 (**2020**), publisher.

(19) Klas, Y. Thesis, High Q nanomechanical resonators fabricated from crystalline silicon carbide (2022).

(20) Huang, X.; Zorman, C.; Mehregany, M., Roukes, M. In *TRANSDUCERS '03. 12th International Conference on Solid-State Sensors, Actuators and Microsystems. Digest of Technical Papers (Cat. No.03TH8664)*, Vol. *1* (IEEE, Boston, MA, USA, 2003), pp 722−725.

(21) Hamelin, B.; Yang, J.; Daruwalla, A.; Wen, H.; Ayazi, F. *Sci. Rep.* **2019**, *9*, 18698.

(22) Xu, M.; Shin, D.; Sberna, P. M.; van der Kolk, R.; Cupertino, A.; Bessa, M. A.; Norte, R. A. *Advanced Materials n/a* **2024**, *36*, 2306513.

(23) Ashby, M. F. *Acta Metall.* **1989**, *37*, 1273.

(24) Schmid, S.; Villanueva, L. G., Roukes, M. L. *Fundamentals of Nanomechanical Resonators* (Springer International Publishing, Cham, 2023).

(25) Ekinci, K. L.; Yang, Y. T.; Roukes, M. L. *J. Appl. Phys.* **2004**, *95*, 2682.

(26) Yang, Y. T.; Callegari, C.; Feng, X. L.; Ekinci, K. L.; Roukes, M. L. *Nano Lett.* **2006**, *6*, 583.

(27) Mauranyapin, N. P.; Romero, E.; Kalra, R.; Harris, G.; Baker, C. G.; Bowen, W. P. *Physical Review Applied 15*, 054036 (**2021**), .

(28) Romero, E.; Mauranyapin, N. P.; Hirsch, T. M.; Kalra, R.; Baker, C. G.; Harris, G. I.; Bowen, W. P. *Physical Review Applied 21*, 054029 (**2024**), .

(29) Villanueva, L.; Schmid, S. *Phys. Rev. Lett.* **2014**, *113*, 227201.

(30) Yasumura, K. Y.; Stowe, T. D.; Chow, E. M.; Pfafman, T.; Kenny, T. W.; Stipe, B. C.; Rugar, D. *J. Microelectromech. S.* *9*, 117 (**2000**).

(31) Norte, R.; Moura, J.; Gröblacher, S. *Phys. Rev. Lett.* **2016**, *116*, 147202.

(32) Forstner, S.; Zych, M.; Basiri-Esfahani, S.; Khosla, K. E.; Bowen, W. P. *Optica* **2020**, *7*, 1427.

(33) Carney, D.; Krnjaic, G.; Moore, D. C.; Regal, C. A.; Afek, G.; Bhave, S.; Brubaker, B.; Corbitt, T.; Cripe, J.; Crisosto, N.; Geraci, A.; Ghosh, S.; Harris, J. G. E.; Hook, A.; Kolb, E. W.; Kunjummen, J.; Lang, R. F.; Li, T.; Lin, T.; Liu, Z.; Lykken, J.; Magrini, L.; Manley, J.;

Matsumoto, N.; Monte, A.; Monteiro, F.; Purdy, T.; Riedel, C. J.; Singh, R.; Singh, S.; Sinha, K.; Taylor, J. M.; Qin, J.; Wilson, D. J.; Zhao, Y., *Quantum Science and Technology* **2021**, *6*, 024002.
(34) Guo, J.; Norte, R.; Gröblacher, S. *Phys. Rev. Lett.* **2019**, *123*, 223602.
(35) Hausmann, B. J. M.; Shields, B.; Quan, Q.; Maletinsky, P.; McCutcheon, M.; Choy, J. T.; Babinec, T. M.; Kubanek, A.; Yacoby, A.; Lukin, M. D.; Lončar, M. *Nano Letters* **2012**, *12*, 1578.
(36) Yang, J.; Van Gasse, K., Lukin, D. M.; Guidry, M. A.; Ahn, G. H.; White, A. D.; Vuckovic, J. *Nature 630*, 853 (**2024**),
(37) Kermany, A. R.; Bennett, J. S.; Brawley, G. A.; Bowen, W. P.; Iacopi, F. *J. Appl. Phys.* **2016**, *119*, 055304.
(38) Schmid, S.; Jensen, K. D.; Nielsen, K. H.; Boisen, A. *Phys. Rev. B* **2011**, *84*, 165307.
(39) Fedorov, S. A.; Engelsen, N. J.; Ghadimi, A. H.; Bereyhi, M. J.; Schilling, R.; Wilson, D. J.; Kippenberg, T. J. *Phys. Rev. B* **2019**, *99*, 054107.
(40) Kimoto, T.; Cooper, J. A. *Fundamentals of Silicon Carbide Technology: Growth, Characterization, Devices and Applications* (John Wiley & Sons, 2014).
(41) Sadeghi, P.; Tanzer, M.; Christensen, S. L.; Schmid, S. *J. Appl. Phys.* **2019**, *126*, 165108.
(42) Islam, M. A.; Alam, M. A.; Shah, M. A. H., Karim, M. M. T. Structural, elastic and electronic properties of 2H- and 4H-SiC. *Int. Journal of Engineering Research and Applications 5* (**2015**).
(43) Jinling Yang; Ono, T.; Esashi, M. *Journal of Micro-electromechanical Systems* **2002**, *11*, 775.
(44) Catalini, L.; Rossi, M.; Langman, E. C.; Schliesser, A. *Phys. Rev. Lett.* **2021**, *126*, 174101.
(45) Tao, Y.; Boss, J. M.; Moores, B. A., Degen, C. L. *Nature Communications 5*, 3638 (**2014**), 1 .
(46) Tao, Y.; Navaretti, P.; Hauert, R.; Grob, U.; Poggio, M.; Degen, C. L. *Nanotechnology* **2015**, *26*, 465501.
(47) Beccari, A.; Visani, D. A.; Fedorov, S. A.; Bereyhi, M. J.; Boureau, V.; Engelsen, N. J.; Kippenberg, T. J. *Nature Physics, 1* (**2022**), 436.
(48) Ghadimi, A. H.; Fedorov, S. A.; Engelsen, N. J.; Bereyhi, M. J.; Schilling, R.; Wilson, D. J.; Kippenberg, T. J. *Science, 6* (**2018**), 764.
(49) Bereyhi, M. J.; Arabmoheghi, A.; Beccari, A.; Fedorov, S. A.; Huang, G.; Kippenberg, T. J.; Engelsen, N. J. *Physical Review X 12*, 021036 (**2022**), .
(50) MacCabe, G. S.; Ren, H.; Luo, J.; Cohen, J. D.; Zhou, H.; Sipahigil, A.; Mirhosseini, M.; Painter, O.*Science370*, 840 (**2020**), .
(51) Bereyhi, M. J.; Beccari, A.; Groth, R.; Fedorov, S. A.; Arabmoheghi, A.; Kippenberg, T. J.; Engelsen, N. J. *Nature Communications 13*, 3097 (**2022**), .
(52) Pratt, J.; Agrawal, A.; Condos, C.; Pluchar, C.; Schlamminger, S.; Wilson, D. *Physical Review X 13*, 011018 (**2023**),.
(53) Cupertino, A.; Shin, D.; Guo, L.; Steeneken, P. G.; Bessa, M. A., Norte, R. A. *Nature Communications 15*, 4255 (**2024**), .
(54) Wang, C.; Fang, Z.; Yi, A.; Yang, B.; Wang, Z.; Zhou, L.; Shen, C.; Zhu, Y.; Zhou, Y.; Bao, R.; Li, Z.; Chen, Y.; Huang, K.; Zhang, J.; Cheng, Y.; Ou, X. *Light: Science & Applications 10*, 139 (**2021**).
(55) Song, B.-S.; Asano, T.; Jeon, S.; Kim, H.; Chen, C.; Kang, D. D.; Noda, S. *Optica 6*, 991 (**2019**), .
(56) Ghyselen, B.; Hartmann, J. M.; Ernst, T.; Aulnette, C.; Osternaud, B.; Bogumilowicz, Y.; Abbadie, A.; Besson, P.; Rayssac, O.; Tiberj, A.; Daval, N.; Cayrefourq, I.; Fournel, F.; Moriceau, H.; Di Nardo, C., Andrieu, F.; Paillard, V.; Cabié, M., Vincent, L.; Snoeck, E.; Cristiano, F.; Rocher, A.; Ponchet, A.; Claverie, A.; Boucaud, P.; Semeria, M. N.; Bensahel, D.; Kernevez, N.; Mazure, C. *Solid-State Electronics Strained-Si Heterostructures and Devices, 48*, 1285 (**2004**).

https://doi.org/10.1021/acs.nanolett.4c06475
Nano Lett. XXXX, XXX, XXX−XXX